Momentum-space interferometry with trapped ultracold atoms

A. Ruschhaupt,[1,*] A. del Campo,[2,3,†] and J. G. Muga[4,‡]
[1]*Institut für Mathematische Physik, TU Braunschweig, Mendelssohnstrasse 3, 38106 Braunschweig, Germany*
[2]*Institute for Mathematical Sciences, Imperial College London, London SW7 2PG, United Kingdom*
[3]*QOLS, The Blackett Laboratory, Imperial College London, Prince Consort Road, London SW7 2BW, United Kingdom*
[4]*Departamento de Química-Física, Universidad del País Vasco, Apartado 644, 48080 Bilbao, Spain*
(Received 9 October 2008; published 12 February 2009)

Quantum interferometers are generally set so that phase differences between paths in coordinate space combine constructively or destructively. Indeed, the interfering paths can also meet in momentum space leading to momentum-space fringes. We propose and analyze a method to produce interference in momentum space by phase imprinting part of a trapped atomic cloud with a detuned laser. For one-particle wave functions analytical expressions are found for the fringe width and shift versus the phase imprinted. The effects of unsharpness or displacement of the phase jump are also studied, as well as many-body effects, to determine the potential applicability of momentum-space interferometry. For a broad range of parameters and conditions it is found that a "dark notch" in the momentum distribution depends linearly on the phase imprinted, with maximal sensitivity for noninteracting atoms in the ground state of tight traps.

DOI: 10.1103/PhysRevA.79.023616 PACS number(s): 37.25.+k, 03.75.Dg, 42.50.−p

I. INTRODUCTION

In most quantum interferometers the phase differential between paths that meet in a coordinate-space point or region at a given time lead to constructive or destructive wave combinations and thus to fringes, but the paths can also interfere in momentum space and produce momentum-space fringes. In particular, during the crossing of a wave packet over a small and thin barrier (compared to the energy and width of the wave packet) [see Fig. 1(a)], the momentum distribution can change dramatically, vanishing at the center of the distribution, and being enhanced at the wings. This process would violate *classical* energy conservation [1], and is due to interference in momentum space between incident and transmitted parts of the wave [2,3].

The experimental implementation of this effect is, in principle, possible with current cold-atom technology, by turning off an effective detuned-laser barrier in the midst of the wave packet passage, but a simpler-to-implement version is described here. The effect of the scattering barrier in the original proposal is to imprint an appropriate phase on approximately half the wave packet, and this can also be achieved by shining part of a trapped, initially stationary, wave packet with a strong laser pulse, during a short time in the scale in which a perturbation propagates (the correlation time [4]) [see Fig. 1(b)]. The phase imprinting technique was first introduced with the purpose of generating vortices [5,6]. Here we shall study the properties of the resulting fringes, and show that the effect on the momentum distribution is similar to the effect of the scattering process, with the creation of a vanishing point ("dark notch") at the center and enhancement of the wings. Furthermore, we shall study the shift, width, and visibility of this central dark notch as a function of the imprinted phase, as a necessary step to determine the potential applicability of momentum-space interferometry as a new tool for quantum metrology. The imprinted phase carries information about the laser interaction (time, laser intensity, frequency) that can be obtained from the notch. We shall see that the notch depends linearly on the phase imprinted in a broad range of parameters and conditions, which allows for a simple interferometric determination of an unknown phase. By immediately removing the external trap, the momentum distribution is essentially frozen after the imprinting, and many-body effects cease to play a role. Then, the momentum-space notch will become by expansion a coordinate-space notch measurable with standard time-of-flight techniques. Alternatively, the momentum distribution can be accessed by stimulated Raman transitions [7] or through the single-particle reduced density matrix [8].

In the following section we will describe the setting in more detail for a single particle or many noninteracting particles. In Sec. III we will consider the role of interactions within the mean-field regime and in Sec. IV we will look at Tonks-Girardeau and noninteracting Fermi gases.

II. NONINTERACTING REGIME

We start considering the noninteracting regime in which the single-particle description is valid. A highly anisotropic three-dimensional harmonic trap is assumed, so that the

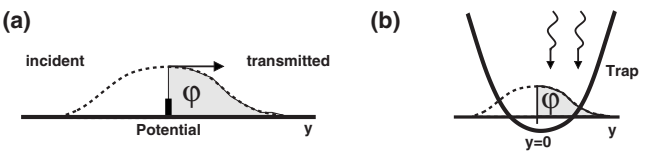

FIG. 1. Schematic settings: (a) Imprinting of a phase φ caused by wave-packet passage above a weak, narrow potential. (b) Phase imprinting caused by illumination with a detuned laser of a wave packet in a harmonic trap.

*a.ruschhaupt@tu-bs.de
†a.del-campo@imperial.ac.uk
‡jg.muga@ehu.es

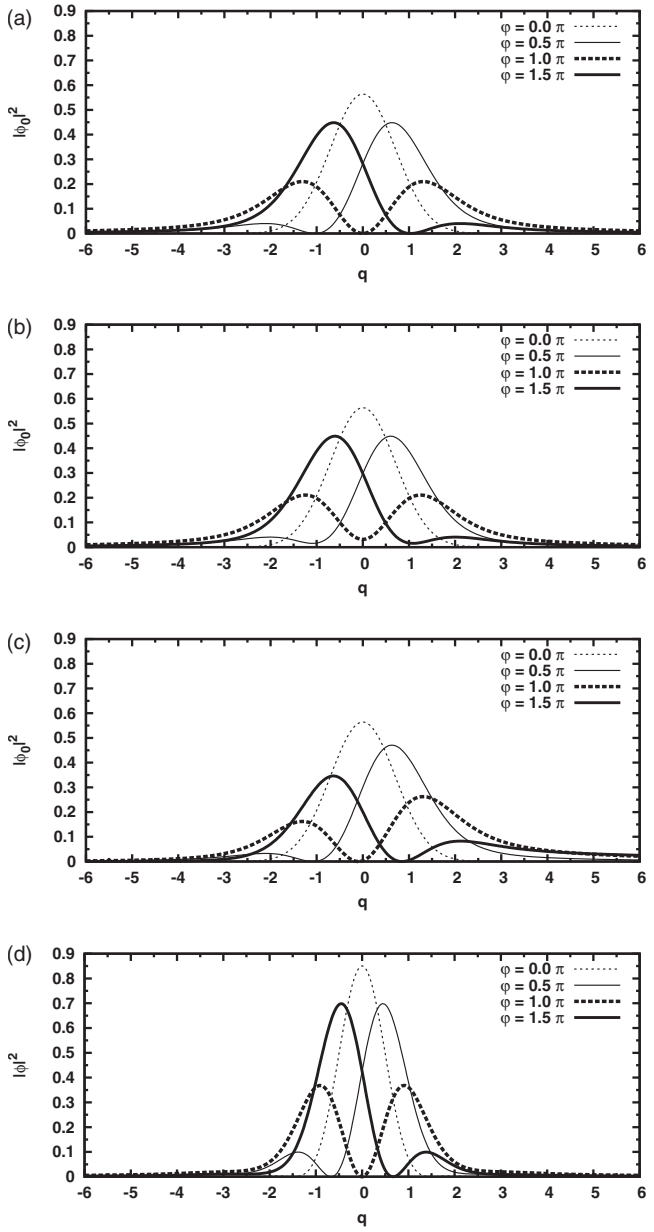

FIG. 2. Momentum probability density for different phase imprintings φ. (a) Reference case (ground state, perfectly sharp, and centered imprinting) $y_0=0$, $\zeta=0$. (b) Effect of shifting the onset of the imprinting, $y_0=0.3$, $\zeta=0$. (c) Effect of smoothing the onset of the imprinting, $y_0=0$, $\zeta=0.1$. (d) Effect of atom-atom interaction, solution of the GPE: $y_0=0$, $\zeta=0$, $g=20$.

transverse degrees of freedom remain frozen and the system becomes effectively one dimensional, along the axis with lowest trap frequency ω. It is useful to introduce dimensionless variables, namely, a dimensionless position $y=\sqrt{\frac{m\omega}{\hbar}}x$, where x is the dimensional position and m is the mass of the single particle, and a dimensionless momentum $q=\sqrt{\frac{\hbar}{m\omega}}k$, where k is the dimensional wave number. The Hamiltonian describing the system is $H=-\frac{\hbar^2}{2m}\frac{\partial^2}{\partial x^2}+\frac{m\omega^2}{2}x^2$ and in the above dimensionless variables we get $H=\frac{\hbar\omega}{2}(-\frac{\partial^2}{\partial y^2}+y^2)$. The corresponding eigenvalues are $E_n=\frac{\hbar\omega}{2}(2n+1)$ and the eigenstates are $\psi_n(y)=\frac{1}{\sqrt{2^n n!}\sqrt{\pi}}H_n(y)e^{-y^2/2}$, where $H_n(y)$ is the nth Hermite polynomial. The eigenstates are normalized such that $\int dy\psi_n(y)\psi_m(y)=\delta_{n,m}$.

Initially, the trapped particle is described by the wave function $\psi_0(y)$ in coordinate space. Then a phase is imprinted on the right-hand side of the trap, i.e., for $y>0$. For atoms, this can be achieved by shining an appropriate detuned laser pulse for a short time t. The detuned laser acts as a mechanical potential $V\Theta(y)$ on the atom, where $V=\Omega^2\hbar/4\Delta$, Ω is the Rabi frequency, and Δ is the detuning (laser frequency minus transition frequency). If the time t is short, the effect is to imprint a phase $\varphi=-Vt/\hbar$ on the wave function for $y>0$. The wave function in coordinate space becomes $\psi_0(y)e^{i\varphi w(y)}$ with $w(y)=\Theta(y)$, and in momentum space

$$\phi_0(q)=\frac{1}{\sqrt{2\pi}}\int_{-\infty}^{0}dy\psi_0(y)e^{-iqy}+e^{i\varphi}\frac{1}{\sqrt{2\pi}}\int_{0}^{\infty}dy\psi_0(y)e^{-iqy}.$$

Each momentum gets an amplitude contribution from two different terms and we may expect interferences in $|\phi_0(q)|^2$ for $\varphi>0$. In the following, this interference pattern will be studied and analytical expressions will be found for the fringe shift, width, and visibility versus the phase φ imprinted. The effects of unsharpness or spatial displacement of the phase jump are also studied.

A. Reference case

Let us first study the effect of imprinting a phase φ on the ground state of the harmonic trap, $n=0$. In this case the momentum probability density becomes

$$|\phi_0(q)|^2=\frac{e^{-q^2}}{\sqrt{\pi}}\left|\cos\left(\frac{\varphi}{2}\right)+\sin\left(\frac{\varphi}{2}\right)\mathrm{erfi}\left(\frac{q}{\sqrt{2}}\right)\right|^2, \quad (1)$$

which has a zero at q_0, a solution of

$$\mathrm{erfi}\left(\frac{q_0}{\sqrt{2}}\right)=-\cot\left(\frac{\varphi}{2}\right). \quad (2)$$

Momentum distributions for this reference case after different phase imprintings are displayed in Fig. 2(a). Note the optimality of $\varphi=\pi$ to produce a deep minimum, in fact a zero, exactly at the peak of the original distribution, $q_0=0$, and the enhancement at the wings. In the following, we will concentrate on this central dark notch. The "motion" of q_0 with φ can be seen in Fig. 2(a), and in more detail in Fig. 3(a) (solid line), where q_0 is plotted versus φ. It shows a linear behavior in $\pi/2<\varphi<3\pi/2$ and slight deviations beyond that range. The width $\Delta q=q_+-q_-$ of the central interference dip is defined as the difference between the momentum q_+ of the maximum on the right-hand side of the minimum and the momentum q_- of the maximum on the left-hand side. Figure 3(b) (solid line) shows the width versus the phase. Note that the width is always greater than $\sqrt{2\pi}$ (value of the thick dotted line).

Another important quantity is the visibility of the minimum, which we define as

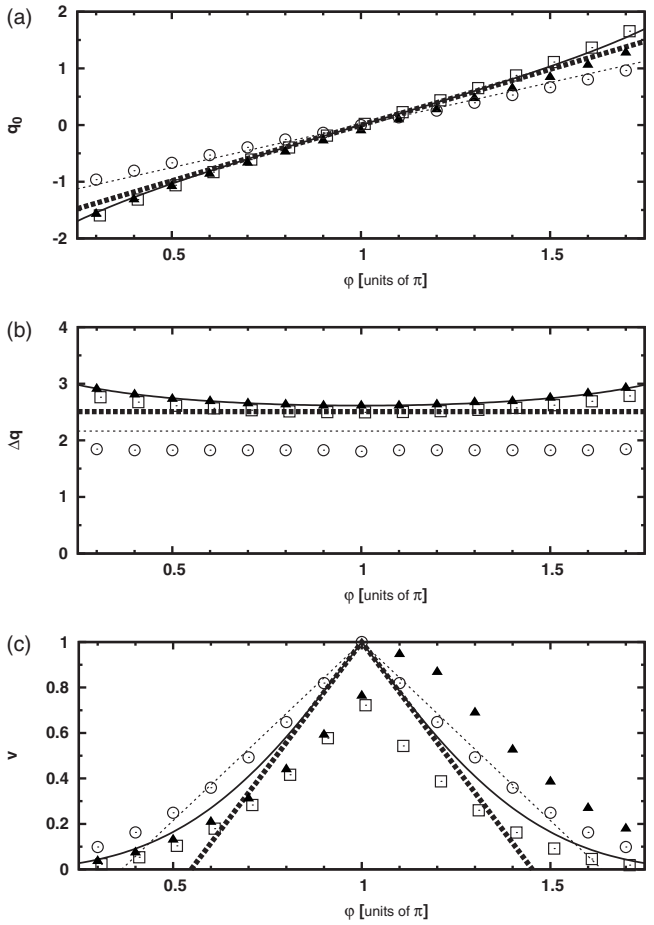

FIG. 3. Momentum interferometry for the ground state $n=0$. (a) Momentum of the minimum of the probability density versus the phase-imprinted φ. (b) Width of the minimum versus φ. (c) Visibility of the minimum versus φ [see Eq. (3)]. Analytical approximations: thick dotted lines, $\tilde{v}$, $\widetilde{\Delta q}$, $\tilde{q}_0$; dotted lines, $\bar{v}$, $\overline{\Delta q}$, $\bar{q}_0$ (Thomas-Fermi with $g=20$). Exact results: Solid line, reference case, v, Δq, q_0 with $y_0=0$, $\zeta=0$, as in Fig. 2(a); boxes, effect of shifting, v, Δq, q_0 with $y_0=0.3$, $\zeta=0$, as in Fig. 2(b); triangles, effect of smoothing, v, Δq, q_0 with $y_0=0$, $\zeta=0.1$, as in Fig. 2(c); circles, effect of interaction, v, Δq, q_0 based on the solution of the GPE with $y_0=0$, $\zeta=0$, $g=20$, as in Fig. 2(d).

$$v = \frac{\min_{\pm}[|\phi_0(q_\pm)|^2 - |\phi_0(q_0)|^2]}{\frac{|\phi_0(q_+)|^2 + |\phi_0(q_-)|^2}{2} + |\phi_0(q_0)|^2}. \tag{3}$$

This visibility is plotted in Fig. 3(c) (solid line). From the calculations we can infer that the visibility limits the working range of the interferometer to $\pi/2 < \phi < 3\pi/2$, and is optimal around $\phi=\pi$.

B. Analytical approximations for the reference case

The goal now is to derive approximate analytical formulas describing the properties of the central dark notch as a function of the imprinted phase. From $\frac{\partial|\phi_0(q)|^2}{\partial q}=0$, we get the extreme points of $|\phi_0(q)|^2$ as solutions of

$$\overbrace{\left[\cos\left(\frac{\varphi}{2}\right)+\sin\left(\frac{\varphi}{2}\right)\mathrm{erfi}\left(\frac{q}{\sqrt{2}}\right)\right]}^{z_1} \times \overbrace{\left\{q\cos\left(\frac{\varphi}{2}\right)-\sin\left(\frac{\varphi}{2}\right)\left[e^{q^2/2}\sqrt{\frac{2}{\pi}}-q\,\mathrm{erfi}\left(\frac{q}{\sqrt{2}}\right)\right]\right\}}^{z_2} = 0. \tag{4}$$

Note that if q is a solution of Eq. (4) for $\varphi=\pi+\Delta\varphi$ then $-q$ is a solution for $\varphi=\pi-\Delta\varphi$.

One of the solutions of Eq. (4) fulfilling $z_1=0$ and describing the momentum of the minimum is approximately given by

$$q_0 \approx \sqrt{\frac{\pi}{2}}\frac{\varphi-\pi}{2} =: \tilde{q}_0 \tag{5}$$

(based on a linearization of $z_1=0$ around $\varphi\approx\pi$ and $q\approx 0$). This describes a linear displacement of the minimum with φ. Figure 3(a) shows the exact momentum of the minimum q_0 (solid line) and $\tilde{q}_0$ (thick dotted line) versus φ.

Now we shall obtain expressions for the (momentum of the) left maximum q_-, and the right maximum q_+. An approximate solution of $z_2=0$ is

$$q_+ \approx \frac{\varphi}{\sqrt{2\pi}} =: \tilde{q}_+,$$

which follows from a linearization of $z_2=0$ around $\varphi\approx 0$ and $q\approx 0$. Another approximate solution of $z_2=0$ is

$$q_- \approx -\frac{2\pi-\varphi}{\sqrt{2\pi}} =: \tilde{q}_-,$$

obtained by linearizing $z_2=0$ around $\varphi\approx 2\pi$ and $q\approx 0$. Thus we get for the width of the interference dip

$$\Delta q = q_+ - q_- \approx \tilde{q}_+ - \tilde{q}_- = \sqrt{2\pi} =: \widetilde{\Delta q}.$$

Figure 3(b) compares the numerically calculated exact width Δq (solid line) with $\widetilde{\Delta q}$ (thick dotted line).

We can also find a simple expression for the visibility. From Eq. (1) and using also the approximations of the momentum of the two maxima and the minima and retaining only the first order in φ we get

$$|\phi_0(q_-)|^2 \approx \alpha+\beta(\varphi-\pi), \quad |\phi_0(q_0)|^2 \approx 0,$$

$$|\phi_0(q_+)|^2 \approx \alpha-\beta(\varphi-\pi),$$

where

$$\alpha = \frac{e^{-\pi/2}}{\sqrt{\pi}}\mathrm{erfi}\left(\frac{\sqrt{\pi}}{2}\right)^2 \approx 0.210,$$

$$\beta = \frac{e^{-\pi/2}}{\pi^{3/2}}\mathrm{erfi}\left(\frac{\sqrt{\pi}}{2}\right)\left[-2e^{\pi/4}+\pi+\pi\,\mathrm{erfi}\left(\frac{\sqrt{\pi}}{2}\right)\right] \approx 0.148.$$

The final result is

$$v \approx 1 - \frac{\beta}{\alpha}|\varphi - \pi| =: \tilde{v},$$

also shown in Fig. 3(c) (thick dotted line). It gives a lower bound for the exact result v (solid line).

C. Perturbations of the reference case

In this subsection we examine the effect of perturbations of the reference case. First we want to discuss the effect of shifting the edge of the phase imprinted region, y_0, out of the center of the trap, i.e., we have $w(z)=\Theta(y-y_0)$. Right after the phase imprinting, the zeroth eigenstate now becomes $\psi_0(y)e^{i\varphi w(z)}=\psi_0(y)e^{i\varphi\Theta(y-y_0)}$, and the momentum distribution becomes

$$|\phi_0(q)|^2 = \frac{e^{-q^2}}{\sqrt{\pi}}\left|\cos\left(\frac{\varphi}{2}\right)+\sin\left(\frac{\varphi}{2}\right)\mathrm{erfi}\left(\frac{q-iy_0}{\sqrt{2}}\right)\right|^2. \quad (6)$$

From $\frac{\partial|\phi_0(q)|^2}{\partial q}=0$, we get the extreme points as solutions of

$$\sqrt{\frac{\pi}{2}}q\exp\left[-\frac{1}{2}(q^2-y_0^2)\right]|z|^2 = \sin\left(\frac{\varphi}{2}\right)\mathrm{Re}(ze^{iqy_0}), \quad (7)$$

where $z=\cos(\frac{\varphi}{2})+\sin(\frac{\varphi}{2})\mathrm{erfi}(\frac{q-iy_0}{\sqrt{2}})$. Again, if q is a solution of Eq. (7) for $\varphi=\pi+\Delta\varphi$ then $-q$ is a solution for $\varphi=\pi-\Delta\varphi$. In addition, Eq. (7) does not change if y_0 is replaced by $-y_0$, so the solutions are the same for $\pm y_0$. If $y_0 \ll 1$, Eqs. (6) and (7) are independent of y_0 to first order in y_0, and therefore the approximations in Sec. II B for the case $y_0=0$ still hold. An example for $y_0=0.3$ is plotted in Fig. 2(b). The corresponding momentum, width, and visibility of the minima versus φ is also plotted in Fig. 3 (boxes). The main effect of increasing y_0 is to lower the visibility [Fig. 3(c)].

Finally, we want to look at the effect of a more realistic smooth profile of the imprinted phase, instead of using an idealized step function. Therefore, we consider now a sigmoid function

$$w(y) = \frac{1}{2}[1+\tanh(y/\zeta)], \quad (8)$$

which for $\zeta \to 0$ becomes $\Theta(y)$. The results for a smoothing $\zeta=0.1$ can be seen in Figs. 2(c) and 3 (triangles). Smoothing results mainly in a shift of the maximum of the visibility [see Fig. 3(c)].

D. Momentum interference for excited states

We shall next consider the effect of phase imprinting on excited states of the harmonic trap with the simplest profile $w(y)=\Theta(y)$. The probability amplitude in momentum space is then given by

$$|\phi_n(q)|^2 = \frac{1}{2\pi 2^n n!\sqrt{\pi}} \times \left|\int_0^\infty dy H_n(y)e^{-y^2/2}[(-1)^n e^{iyq}+e^{i\varphi}e^{-iyq}]\right|^2,$$

which clearly simplifies for $n=0$ to Eq. (1).

Let us look for q_0 fulfilling $|\phi_n(q_0)|^2=0$, i.e., for the momentum of the minimum. Assuming $q_0 \ll 1$ such that $(-1)^n e^{iyq_0}+e^{i\varphi}e^{-iyq_0} \approx [(-1)^n+e^{i\varphi}]+iq_0[(-1)^n-e^{i\varphi}]y$,

$$|\phi_n(q_0)|^2 \approx \frac{1}{2\pi 2^n n!\sqrt{\pi}} \times |[(-1)^n+e^{i\varphi}]A_n + iq_0[(-1)^n-e^{i\varphi}]B_n|^2,$$

where we have introduced $A_n=\int_0^\infty dy H_n(y)e^{-y^2/2}$, and $B_n=\int_0^\infty dy y H_n(y)e^{-y^2/2}$. Solving this for $|\phi_n(q_0)|^2=0$, we get

$$q_0 \approx i\frac{(-1)^n+e^{i\varphi}}{(-1)^n-e^{i\varphi}}\frac{A_n}{B_n}. \quad (9)$$

The cases in which n is even or odd will be examined separately.

(*a*) *n even*. We are interested in the motion of the zero $|\phi_n(q_0)|^2=0$ for $\varphi \approx \pi$. From Eq. (9) we get in first order in $\varphi-\pi$ that

$$q_0 \approx \frac{A_n}{B_n}\frac{\varphi-\pi}{2} =: \tilde{q}_0.$$

Examples for the exact solution q_0 and the approximation $\tilde{q}_0$ for $n=0,2$ can be found in Fig. 4(a).

(*b*) *n odd*. Now we are interested in the motion of the zero $|\phi_n(q_0)|^2=0$ versus φ for $\varphi \approx 0$. From Eq. (9) we get in first order in φ that

$$q_0 \approx \frac{A_n}{B_n}\frac{\varphi}{2} =: \tilde{q}_0.$$

Examples for the exact solution q_0 and the approximation $\tilde{q}_0$ for $n=1,3$ can be found in Fig. 4(b).

In addition, Fig. 4(c) shows the value of the ratio $\frac{A_n}{B_n}$ for odd and even n. Clearly, increasing n makes the interferometer less sensitive to phase variations and $n=0$ provides the optimal behavior.

III. MEAN-FIELD REGIME

We shall consider now the role of the interactions within the mean-field approach. In the mean-field regime, for low enough temperatures the phase fluctuations can be suppressed [9]. Weakly interacting ultracold gases in one dimension (1D) are then described by the Gross-Pitaevskii equation (GPE).

Assume that an effectively 1D Bose-Einstein condensate is prepared in the harmonic trap. The condensate wave function is the ground state of the 1D (stationary) GPE

$$\mu\Psi(x) = -\frac{\hbar^2}{2m}\frac{\partial^2\Psi(x)}{\partial x^2}+\frac{m\omega^2}{2}x^2\Psi(x)+\frac{\hbar}{2}g_{1\mathrm{D}}|\Psi(x)|^2\Psi(x),$$

where μ is the chemical potential and $g_{1\mathrm{D}}$ is the effective 1D

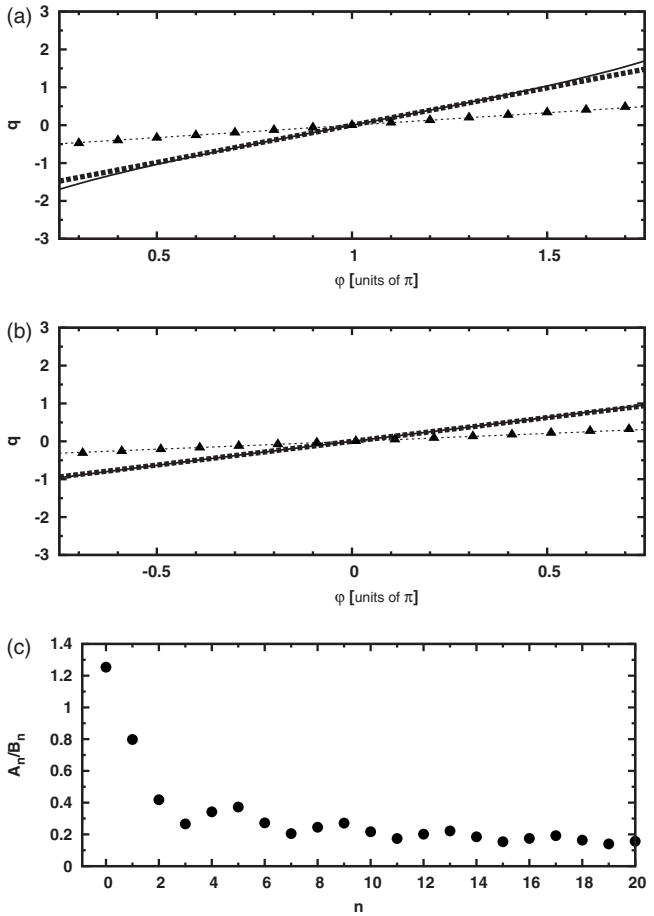

FIG. 4. Momentum interferometry for excited states. [(a) and (b)] Momentum of minimum versus φ. (a) $n=0$: exact value q_0 (solid line), approximation $\tilde{q}_0$ (thick dotted line); $n=2$: q_0 (triangles), $\tilde{q}_0$ (dotted line). (b) $n=1$: q_0 (solid line), $\tilde{q}_0$ (thick dotted line); $n=3$: q_0 (triangles), $\tilde{q}_0$ (dotted line). (c) Ratio $\frac{A_n}{B_n}$ versus n showing loss of sensitivity.

coupling parameter related to the three-dimensional scattering length [10]. We assume that $\int dx|\Psi(x)|^2=1$. By introducing $u:=2\mu/(\hbar\omega)$, $g:=\sqrt{\frac{m}{\hbar\omega}}g_{1D}$, and $\psi(y):=\sqrt[4]{\frac{\hbar}{m\omega}}\Psi(\sqrt{\frac{\hbar}{m\omega}}y)$ we can write this equation in dimensionless form,

$$u\psi(y) = -\frac{\partial^2\psi(y)}{\partial y^2} + y^2\psi(y) + g|\psi(y)|^2\psi(y),$$

with $\int dy|\psi(y)|^2=1$. The ground state can be numerically computed by using the imaginary time method [11,12]. For $\varphi=0$, it is well known that as the mean-field interaction is increased, the density profile becomes more uniform, while the resulting momentum distribution $|\phi|^2$ is sharply peaked [13,14]. To study the effect of a small g as a perturbation of

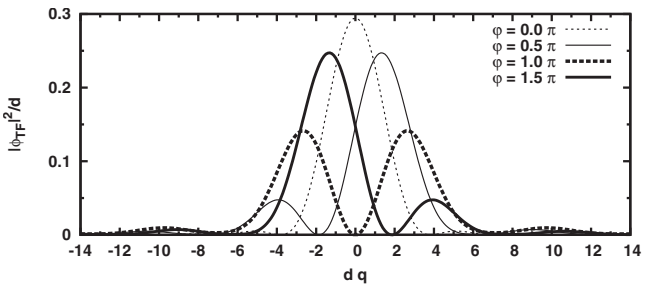

FIG. 5. Interference in the momentum distribution of a Bose-Einstein condensate in the Thomas-Fermi regime and for different phases φ imprinted.

the previous results, we shall imprint a phase φ on the ground-state wave function and calculate the minimum of the resulting interference pattern in momentum space. An example with $g=20$ is shown in Fig. 2(d). The visibility, the width, and the momentum of the minimum versus φ with $g=20$ is shown in Fig. 3 (circles). The main effect is that the slope in Fig. 3(b) decreases with increasing atom-atom interaction, i.e., the sensitivity of the interferometer with respect to φ decreases with increasing g. A large atom-atom interaction g may also perturb the measurement of the momentum distribution by time-of-flight techniques. There is, however, also a positive effect: an increase of g makes the interference dip sharper and improves the visibility [see Fig. 3(c)].

It is possible to derive analytical approximate formulas for large g. For $g\gg 1$ the condensate enters into the Thomas-Fermi regime [13,14]. The mean-field interaction is then so large that the kinetic energy can be neglected in the Hamiltonian so that the time-independent GPE reads $u\psi(y)=(y^2+g|\psi(y)|^2)\psi(y)$. The Thomas-Fermi wave function is then given by $\psi_{TF}(y)=\sqrt{(u-y^2)/g}$ with $u=(3g/4)^{2/3}$ whenever $|y|<d$ and zero elsewhere; $d=\sqrt{u}$ is the Thomas-Fermi half-width.

The probability distribution in momentum space after a phase imprinting φ with a profile $w(y)=\Theta(y)$ is given in this case by

$$|\phi_{TF}(q)|^2 = \frac{3\pi}{8dq^2}\left[J_1(qd)\cos\left(\frac{\varphi}{2}\right) + \mathbf{H}_1(qd)\sin\left(\frac{\varphi}{2}\right)\right]^2. \tag{10}$$

Here, $J_1(k)$ is the Bessel function of first order and $\mathbf{H}_1(y)$ is the first order Struve function [15]. $|\phi_{TF}(q)|^2/d$ is plotted for different values of φ in Fig. 5. Again there is a minimum for $\varphi=\pi$ at $q=0$, which is shifted if φ is changed.

The minima and the maxima of $|\phi_{TF}(q)|^2$ for a fixed φ can be found by looking at the zeros of the derivative, this leads to the equation

$$\underbrace{\frac{1}{qd}\left[J_1(qd)\cos\left(\frac{\varphi}{2}\right) + \mathbf{H}_1(qd)\sin\left(\frac{\varphi}{2}\right)\right]}_{a_1}\underbrace{\frac{1}{(qd)^2}\left\{\pi qdJ_2(qd)\cos\left(\frac{\varphi}{2}\right) + \left[2 + \pi qd\mathbf{H}_{-2}(qd)\sin\left(\frac{\varphi}{2}\right)\right]\right\}}_{a_2} = 0.$$

Making $a_1=0$ and using a linearization around $q\approx 0$ and $\varphi \approx \pi$, we arrive at

$$q \approx \frac{3\pi}{8d}(\varphi - \pi) =: \bar{q}_0,$$

where $d=(3g/4)^{1/3}$, which allows one to find d measuring the notch displacement. Making $a_2=0$ and using a linearization around $q\approx 0$ and $\varphi\approx 0$, we arrive at

$$q \approx \frac{8}{3\pi d}\varphi =: \bar{q}_+,$$

and by using a linearization around $q\approx 0$ and $\varphi\approx 2\pi$, we arrive at

$$q \approx -\frac{8}{3\pi d}(2\pi - \varphi) =: \bar{q}_-.$$

An estimate of the width is then $\overline{\Delta q}=\bar{q}_+-\bar{q}_-=\frac{16}{3d}$. An approximation for the visibility can also be derived as in Sec. II B,

$$v \approx 1 - 0.5|\varphi - \pi| =: \bar{v}.$$

The approximate values of the notch momentum, width, and visibility in the Thomas-Fermi regime are also plotted in Fig. 3 (dotted lines).

IV. TONKS-GIRARDEAU AND NONINTERACTING FERMI GASES

At low enough densities, and under tight-transverse confinement, ultracold gases enter the Tonks-Girardeau (TG) regime [16], in which the strength of the effective short-range interactions becomes so large that the mean-field theory fails [17]. Fortunately, Bose-Fermi duality offers a powerful and exact approach, exploiting the similarities between the TG and spin-polarized noninteracting Fermi gases. The ground-state wave function of the latter in a harmonic trap is the familiar Slater determinant $\Psi_F(y_1,\ldots,y_N)=\frac{1}{\sqrt{N!}}\det_{n,k=(0,1)}^{(N-1,N)}\psi_n(y_k)$, built from the set of single-particle orthonormal eigenstates $\{\psi_n(y)\}$. Such an atom Fock state can be efficiently prepared using the atom culling technique as described in [18,19]. Note that the wave function Ψ_F is totally antisymmetric and vanishes whenever the positions of two particles coincide. The TG wave function is obtained from Ψ_F by imposing the correct symmetry under permutation of particles, i.e., using the Fermi-Bose (FB) mapping [16]

$$\Psi_{TG}(y_1,\ldots,y_N) = \prod_{1\leqslant j<k\leqslant N} \mathrm{sgn}(y_k - y_j)\Psi_F(y_1,\ldots,y_N).$$

Clearly, both dual systems share the same density profile [17] $\rho_{TG/F}(y,t)=N\int|\Psi_{TG/F}(y,y_2,\ldots,y_N;t)|^2dy_2\cdots dy_N=\Sigma_{n=0}^{N-1}|\psi_n(y,t)|^2$, as is the case for any other local correlation function. However, their momentum distributions

$$n(q) = (2\pi)^{-1}\int dy\, dy' e^{iq(y-y')}\rho(y,y') \tag{11}$$

are drastically different. Provided that the reduced single-particle density matrix (RSPDM) of spin-polarized fermions is

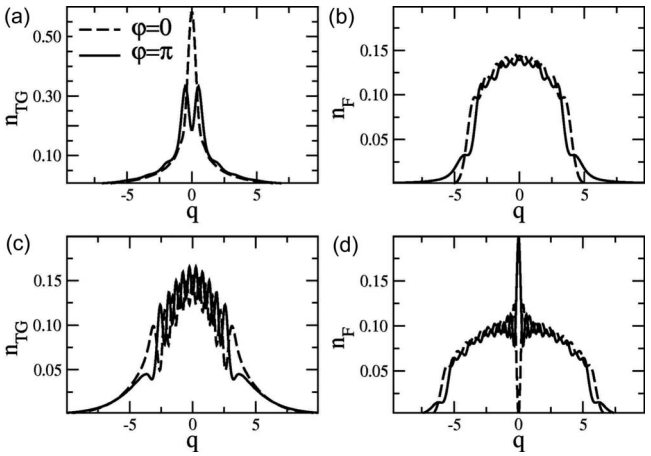

FIG. 6. Interference in momentum space, $N=10$, a $\varphi=\pi$ phase is imprinted for $y>0$ (solid line); the momentum distribution for $\varphi=0$ is also depicted (dashed line). (a) TG gas. (b) Fermi gas. (c) TG gas after parity-selective evaporation. (d) Fermi gas after parity-selective evaporation.

$$\rho_F(y,y') = \sum_{n=0}^{N-1}\psi_n^*(y)\psi_n(y'), \tag{12}$$

the momentum distribution is the sum $n_F(q)=\Sigma_{n=0}^{N-1}|\tilde{\psi}_n(q)|^2$ (where $\tilde{\psi}_n$ denotes the Fourier transform of ψ_n). For the TG gas, an efficient way of computing the RSPDM has been introduced [20,21], namely,

$$\rho_{TG}(y,y') = \sum_{l,n=0}^{N-1}\psi_l^*(y)A_{ln}(y,y')\psi_n(y'), \tag{13}$$

where $\mathbf{A}(y,y')=(\mathbf{P}^{-1})^T\det\mathbf{P}$ and the elements of the matrix $\mathbf{P}$ are $P_{ln}(y,y')=\int dz\,\psi_l^*(z)\phi_n(z)\mathrm{sgn}(z-y)\mathrm{sgn}(z-y')$, which reduces to $P_{ln}=\delta_{ln}-2\int_y^{y'}dz\,\psi_l^*(z)\phi_n(z)$ for $y<y'$ without loss of generality. The momentum distribution of the TG gas can thus be obtained as a double Fourier transform.

We consider a phase imprinting with $w(y)=\Theta(y)$. Under this phase imprinting, a remarkable difference arises between the momentum distribution of both dual systems. For a moderate N the visibility of the interference fringes in the TG gas is reduced [see Fig. 6(a)] but in the fermionic case the pattern has been washed out completely [see Fig. 6(b)]. For larger N the visibility of the TG dip decreases. It is hence clear that the observation of such effect in any of these dual systems would be difficult, and we turn our attention to a closely related alternative approach.

Recently, a parity-selective evaporation (PSE) method has been proposed, which allows one to prepare, in principle, excited states composed exclusively of odd-parity single-particle eigenstates [22]. This is achieved by shining a blue-detuned laser at $y\sim 0$, which removes the even-parity eigenstates. For a spin-polarized Fermi gas the excited many-body wave function becomes $\Psi_F(y_1,\ldots,y_N)=\frac{1}{\sqrt{N!}}\det_{n,k=1}^{N}\psi_{2n-1}(y_k)$. The corresponding momentum distribution exhibits a well-defined zero at $q=0$ for all N which is stationary, and robust against significant smoothing of the

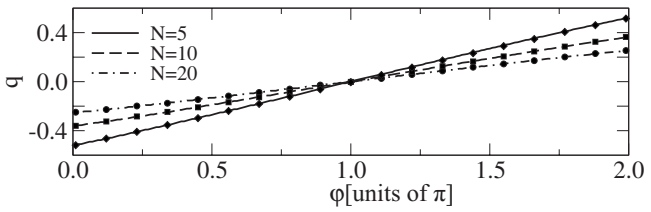

FIG. 7. Displacement of the maximum of the momentum distribution as a function of the phase imprinted, for parity-selective evaporation, and a fermionic cloud with only odd states. The symbols correspond to a smooth phase-imprinting profile with $\zeta=1/2$, whereas for the lines $\zeta=0$.

phase-imprinting profile. The TG wave function equally follows from the Bose-Fermi map for PSE-prepared states. However, the $n_{TG}(q)$ is qualitatively insensitive to the selected parity of the single-particle states, and lacks any principal peak (or dip) potentially useful for momentum-space interferometry [see Fig. 6(c)]. On the other hand, the pattern $n_F(q)$ in the fermionic case is reversed under phase imprinting, turning a zero into a peak in the momentum distribution [see Fig. 6(d)]. Let us consider again a phase imprinting with the sigmoid profile (8). In Fig. 7 we have calculated the shift of the maximum in $n_F(q)$ as a function of φ for the cases $\zeta=0$ (Heaviside function) and $\zeta=0.5$. The dependence is found to be linear even in the presence of the large smoothing in the profile $\zeta=0.5$.

Therefore, between both dual systems the TG gas is preferred using phase imprinting, whereas in combination with PSE, the fermionic system is a better candidate.

V. DISCUSSION

The localized phase-imprinting method [4] on trapped cold atoms has been discussed up to now mostly in connection with the generation and study of solitons. In this paper we have instead focused on the characterization of the momentum distribution right after the phase imprinting.

First, phase imprinting of half the wave packet can be regarded as a simple way to realize the interferometry in momentum space that has been previously put forward for more complex scattering processes between cold atoms and weak laser barriers [1–3]. Similar to the scattering setting, a central dark notch appears in the momentum distribution after phase imprinting, as well as an enhancement of the wings. An advantage with respect to the scattering method is that there is no need to make the momentum width of the incident wave packet small to get the same transmission coefficient and therefore the same phase shift for all momenta. Thus we can make the trap tighter and tighter increasing the sensitivity.

Furthermore, the characterization of the momentum distribution is a preliminary step to determine the potential applicability of momentum interferometry where an unknown phase should be determined from the momentum shift of the central dark notch.

We have studied different configurations, regimes, and perturbations. The momentum dark notch for noninteracting particles in the ground state provides the most sensitive meter for the imprinted phase among the different states considered. In dimensionless units, the momentum of the dark notch versus the imprinted phase is in this case given by $\tilde{q}_0=\sqrt{\frac{\pi}{2}}\frac{\varphi-\pi}{2}$ [see Eq. (5)]. In dimensional units we get for the corresponding velocity

$$\tilde{v}_0=\sqrt{\frac{\hbar\omega}{m}}\left(\frac{\pi}{2}\right)^{3/2}\frac{\varphi-\pi}{\pi},$$

such that we can enhance the sensitivity to phase differences, in principle, to arbitrarily high values by increasing ω. If the external trap is immediately removed after the phase imprinting, the momentum distribution is essentially frozen and the velocity $\tilde{v}_0$ can be measured with a standard time-of-flight technique. Assuming a free time of flight of duration t after the phase imprinting, the dark notch will move a distance $\tilde{s}_0=t\tilde{v}_0$. If the spatial resolution is Δs, the resolvance r of the momentum interferometer can be defined for the reference case as

$$r:=\frac{\pi}{\Delta\varphi}=\frac{t}{\Delta s}\sqrt{\frac{\hbar\omega}{m}}\left(\frac{\pi}{2}\right)^{3/2},$$

where $\Delta\varphi$ is the minimum resolvable deviation of the phase from π. For $t=200$ ms, $m=\text{mass}(^{87}\text{Rb})$, $\omega=2\pi\times 2$ kHz and $\Delta s=5$ μm, we get $r\approx 239$. The effects of unsharpness or spatial displacement of the phase jump have also been studied and the results qualitatively still hold. Many-body effects in the mean-field regime lead to a mild sensitivity loss but also to an interesting increase of visibility. In all cases there is still a linear dependence of the dark notch velocity on the phase φ, i.e., $\tilde{v}_0\propto\varphi-\pi$ such that the phase can be determined from the velocity of the dark notch.

Other extreme regimes, such as the Tonks-Girardeau gas of bosons or an ideal Fermi gas diminish the interference, except, in the latter case, when an auxiliary parity-selection procedure is applied to retain odd states. A peak is then formed with linear dependence on the imprinted phase, very stable with respect to the smoothness of the profile of the imprinting laser.

Finally, note that even though there are no atom-atom interactions in the reference case, some of the aspects usually attributed to the solitons may already be recognized, in particular, the formation of the dark notch in momentum representation and its shift with the value of the phase jump or its smoothness. Dynamical studies of the state evolution will provide further comparison with soliton dynamics and will be dealt with elsewhere.

ACKNOWLEDGMENTS

We acknowledge fruitful conversations with M. Siercke, C. Ellenor, and A. Steinberg. We further acknowledge "Acciones Integradas" of the German Academic Exchange Service (DAAD) and Ministerio de Educación y Ciencia, and additional support from the Max Planck Institute for the Physics of Complex Systems, MEC (Grant No. FIS2006-10268-C03-01), and UPV-EHU (Grant No. GIU07/40). A.R. acknowledges support by the German Research Foundation (DFG) and the Joint Optical Metrology Center (JOMC, Braunschweig).

[1] S. Brouard and J. G. Muga, Phys. Rev. Lett. **81**, 2621 (1998).
[2] A. L. Pérez Prieto, S. Brouard, and J. G. Muga, Phys. Rev. A **64**, 012710 (2001).
[3] A. L. Pérez Prieto, S. Brouard, and J. G. Muga, Phys. Rev. A **71**, 012703 (2005).
[4] K. Bongs and K. Sengstock, Rep. Prog. Phys. **67**, 907 (2004).
[5] L. Dobrek, M. Gajda, M. Lewenstein, K. Sengstock, G. Birkl, and W. Ertmer, Phys. Rev. A **60**, R3381 (1999).
[6] B. P. Anderson, P. C. Haljan, C. A. Regal, D. L. Feder, L. A. Collins, C. W. Clark, and E. A. Cornell, Phys. Rev. Lett. **86**, 2926 (2001).
[7] M. D. Girardeau and E. M. Wright, Phys. Rev. Lett. **87**, 050403 (2001).
[8] I. Bloch, T. W. Hänsch, and T. Esslinger, Nature (London) **403**, 166 (2000).
[9] D. M. Gangardt and G. V. Shlyapnikov, Phys. Rev. Lett. **90**, 010401 (2003).
[10] M. Olshanii, Phys. Rev. Lett. **81**, 938 (1998); V. Dunjko, V. Lorent, and M. Olshanii, *ibid.* **86**, 5413 (2001).
[11] M. M. Cerimele, M. L. Chiofalo, F. Pistella, S. Succi, and M. P. Tosi, Phys. Rev. E **62**, 1382 (2000).
[12] M. L. Chiofalo, S. Succi, and M. P. Tosi, Phys. Rev. E **62**, 7438 (2000).
[13] G. Baym and C. J. Pethick, Phys. Rev. Lett. **76**, 6 (1996).
[14] F. Dalfovo, L. Pitaevskii, and S. Stringari, Phys. Scr., T **T66**, 234 (1996).
[15] A. Abramowitz and I. A. Stegun, *Handbook of Mathematical Functions* (Dover, New York, 1965).
[16] M. Girardeau, J. Math. Phys. **1**, 516 (1960).
[17] M. D. Girardeau and E. M. Wright, Phys. Rev. Lett. **84**, 5239 (2000).
[18] A. M. Dudarev, M. G. Raizen, and Q. Niu, Phys. Rev. Lett. **98**, 063001 (2007).
[19] A. del Campo and J. G. Muga, Phys. Rev. A **78**, 023412 (2008).
[20] R. Pezer and H. Buljan, Phys. Rev. Lett. **98**, 240403 (2007).
[21] H. Buljan, K. Lelas, R. Pezer, and M. Jablan, Phys. Rev. A **76**, 043609 (2007).
[22] H. Buljan, O. Manela, R. Pezer, A. Vardi, and M. Segev, Phys. Rev. A **74**, 043610 (2006).